High Energy Density Physics 23 (2017) 129–132

Contents lists available at ScienceDirect

High Energy Density Physics

journal homepage: www.elsevier.com/locate/hedp

The creation of radiation dominated plasmas using laboratory extreme ultra-violet lasers

G.J. Tallents*, S. Wilson, A. West, V. Aslanyan, J. Lolley, A.K. Rossall

York Plasma Institute, Department of Physics, University of York, York YO10 5DD, UK

ARTICLE INFO

Article History:
Received 21 March 2017
Accepted 30 March 2017
Available online 31 March 2017

Keywords:
Warm dense matter
Degenerate plasma
Spectroscopy
Extreme ultra-violet

ABSTRACT

Ionization in experiments where solid targets are irradiated by high irradiance extreme ultra-violet (EUV) lasers is examined. Free electron degeneracy effects on ionization in the presence of a high EUV flux of radiation is shown to be important. Overlap of the physics of such plasmas with plasma material under compression in indirect inertial fusion is explored. The design of the focusing optics needed to achieve high irradiance (up to 10^{14} Wcm^{-2}) using an EUV capillary laser is presented.

1. Introduction

The extreme ultra-violet (EUV) spectral range (10–100 nm) has significant potential for a number of applications. EUV radiation is being used to expose photo-resist for the latest generation of computer chip manufacture [1] and purpose-built free electron lasers operating in the EUV have been constructed [2,3]. A useful laboratory scale laser operating in the EUV at wavelength 46.9 nm has been developed by Rocca et al.[4,5]. This 46.9 nm laser creates output by compressing argon plasma in a capillary confined *Z*-pinch arrangement. Lasing from Ne-like argon ions on a 3p-3s ($J = 0-1$) transition occurs by amplified spontaneous emission with laser output up to 1 mJ energy in pulses of typically 1.5 ns.

The use of EUV lasers for the ablation of small-scale features in solids has been explored [6,7]. The diameter d_R of a focused laser beam is determined by the wavelength λ of the radiation and the numerical aperture N_A of the focusing optic such that

$$d_R = C_f \frac{\lambda}{N_A} \quad (1)$$

where C_f is a constant varying with the intensity and phase profile of the focused laser beam with a minimum diffraction limited value of $C_f = 2/\pi = 0.64$ for a Gaussian beam. A narrow focus can be formed using EUV lasers due to the combination of the short wavelength of EUV radiation and the ability to create optics with large numerical aperture based on multi-layer mirrors. As well as enabling the ablation of small features for applications, reducing the diameter of beam focus enables higher irradiances to be produced. Harder x-rays typically need to be focused using grazing-incidence optics which limits the maximum numerical aperture possible and the size of focus to a diffraction limited diameter of ≈ 1.5 μm [8]. EUV irradiances from capillary lasers are now comparable to some optical laser experiments ($> 10^{10}$ Wcm^{-2}, see [9]), with the potential to achieve irradiances up to 10^{14} Wcm^{-2} with optimised focusing.

The plasma formed by lower irradiance ($<10^{11}$ Wcm^{-2}) EUV capillary laser irradiation of solid targets has been investigated [7,9–11]. The critical electron density for EUV wavelengths in the range 10–100 nm ranges from $10^{25}-10^{23}$ cm^{-3}. Ionised solid materials consequently have electron densities below the critical density, so that the EUV laser light penetrates through ablated, expanding plasma material and can interact directly with material at solid density. Absorption by direct photo-ionization as well as inverse bremsstrahlung occurs. The laser energy is deposited over a longer spatial range and energy deposition is not concentrated near the critical density as occurs with optical laser interactions. Consequently, a greater mass/unit area of material is ablated. With the laser energy spread over a greater mass of material, the temperatures achieved are lower than for optical laser interactions, with significant mass of material at solid density. An EUV laser produces a volume of warm dense matter which during the laser irradiation has a large flux of incoming radiation (the EUV laser itself).

Indirect drive inertial fusion seeks to produce plasma in the pellet shell and fuel at high density and moderate temperature which is irradiated by a high flux of radiation from within the hohlraum [12]. We are seeking to explore the parallels between the plasmas created in indirect drive inertial fusion and in EUV laser interaction with solids. We have shown that the free electron degeneracy has a

* Corresponding author.
E-mail address: greg.tallents@york.ac.uk (G.J. Tallents).

http://dx.doi.org/10.1016/j.hedp.2017.03.010
1574-1818/

dominant role in changing the ionization of plasmas created by EUV radiation if the radiation intensity is sufficiently intense ($>10^{14}$ Wcm^{-2} [13]). In this paper, we first examine the effects on plasma ionization likely to be observed when photo-ionization dominates the creation of plasma material and then explore some of the experimental issues in creating radiation dominated plasma using capillary laser irradiation of solids.

2. The effects of free electron degeneracy on collisional and radiative processes

We first examine the rates of photo-ionization and three-body recombination in warm dense plasmas. The free electron quantum states can become close to fully occupied which means that the electron energy distribution is given by the Fermi–Dirac distribution rather than a Maxwellian distribution. The full occupancy of free electron quantum states also means that transition rates may be reduced as electrons cannot transition to occupied free electron quantum states. We reduce the transition rates due to electron occupancy by multiplying the necessary cross-sections or rate coefficients by blocking factors of form unity minus the occupancy of the final free electron quantum state.

If the density is high and the temperature of a plasma is low, the chemical potential associated with the near-full occupancy of free electron quantum states is important. The chemical potential of the free electrons is the energy required to add another electron per unit volume to the free electrons. The chemical potential is found, in practise, by integrating the Fermi–Dirac distribution containing the relevant chemical potential, so that the total number of free electrons in unit volume is correct.

As the chemical potential μ is related to the electron density by the requirement that an integration of the electron distribution function over all energies gives the total free electron density n_e, we can write

$$n_e = \int_0^\infty f_{FD}(E)dE = \frac{4}{\sqrt{\pi}}\left(\frac{2\pi m_0 kT}{h^2}\right)^{3/2} I_{1/2}(\mu/kT) \tag{2}$$

where $I_m(\eta_C)$ is the Fermi–Dirac integral of order m. We introduce a reduced chemical potential $\eta_C = \mu/kT$ and write for the Fermi–Dirac integral

$$I_m(\eta_C) = \int_0^\infty \frac{x^m dx}{\exp(x-\eta_C)+1}. \tag{3}$$

The reduced chemical potential $\eta_C = \mu/kT$ can be determined using Eq. (2). We plot a scaling of electron density and temperature as a function of the reduced chemical potential η_C (see Fig. 1). The vertical axis of Fig. 1 corresponds to constant adiabats.

For indirect drive inertial fusion design studies, the pressure of the imploding fuel relative to the Fermi pressure of degenerate electrons is kept below 1.7 [14] which corresponds to a reduced chemical potential $\eta_C > 1.5$ (see [15]) . For EUV laser-plasmas, we can deduce the chemical potential range from Fig. 1. Assuming an ionization of Z_{av} per atom and that plasma is formed at material density ρ in units of g cm^{-3}, the electron density in cm^{-3} is given by

$$n_e = \frac{\rho Z_{av}}{1.67A} \times 10^{24} \tag{4}$$

where A is the atomic mass of the target material. Eq. (4) and Fig. 1 show that it is relatively straightforward to create high density plasma material using an EUV laser focused onto a solid target which exhibits a reduced chemical potential in the range of interest for indirect drive inertial fusion. Many elements at room temperature have $\rho/A > 1/6$ g cm^{-3} suggesting from Eq. (4) that their use as targets for EUV laser ablation can enable electron densities of $n_e \approx 10^{23}$ cm^{-3} with $Z_{av} \approx 1$. For electron temperatures $kT < 20$ eV, the corresponding reduced chemical potential $N_C > 1.5$. This is the same desired chemical potential range as required for indirect drive inertial fusion.

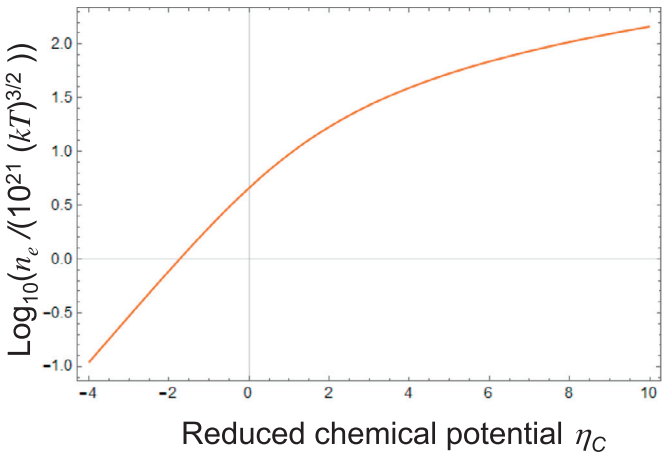

Fig. 1. The scaling of electron density n_e in units of cm^{-3} and electron temperature kT in units of eV as a function of the reduced chemical potential $\eta_C = \mu/kT$. At negative chemical potential, the free electron degeneracy is not significant and there is log linear variation.

2.1. Collisional ionization and three-body recombination

A collisional ionization rate coefficient K_{ion} evaluation requires a knowledge of the differential cross-section $\sigma(E, E_1)$ where we assume, say, that the incident electron has an energy E and the ejected electrons have energy E_1 and $E_2 = E - E_1 - E_{ion}$. We can write [15] that

$$K_{ion}N_e = \int_{E_{ion}}^\infty \left(\frac{2E}{m}\right)^{1/2} f(E)\left[\frac{\int_0^{E-E_{ion}} \sigma(E,E_1)\ P(E_1)\ P(E_2)\ dE_1}{\int_0^{E-E_{ion}} dE_1}\right] dE \tag{5}$$

where the blocking factors $P(E_1)$ and $P(E_2)$ are appropriate for the two ejected electrons. We assume that the initial bound state has an ionization energy of E_{ion}. The integrations in the square bracket average the differential cross-section and blocking factors over the range of ejected electron energies (from zero energy to the impinging electron energy minus the ionization energy).

We can assume for an approximate treatment that the differential cross-section is constant with ejected electron energy E_1 and simply varies as $\sigma(E,E_1) = \sigma(E_{ion},0)E_{ion}/E$. With the assumption that the differential cross-section is independent of the energy distribution between the two electrons, the rate coefficient can be written as

$$K_{ion}N_e \approx \frac{4}{\sqrt{\pi}}\left(\frac{2\pi m}{h^2}\right)^{3/2}\left(\frac{2}{m}\right)^{1/2} E_{ion}\ \sigma(E_{ion},0)\ J_{ion}(E_{ion})\ kT \tag{6}$$

with

$$J_{ion}(E_{ion}) = \int_{E_{ion}}^\infty \frac{1}{\exp\left(-\frac{\mu-E}{kT}\right)+1}\ \frac{1}{E-E_{ion}} I_{in}\, dE \tag{7}$$

and

$$I_{in} = \int_0^{\frac{E-E_{ion}}{kT}} \left(1-\frac{1}{\exp\left(-\frac{\mu-E_1}{kT}\right)+1}\right)\left(1-\frac{1}{\exp\left(-\frac{\mu-E_2}{kT}\right)+1}\right) d\left(\frac{E_1}{kT}\right). \tag{8}$$

The inner integral I_{in} is over the blocking factors for the two electrons after the collision. For non-degenerate free electrons, the solution of Eq. (7) is

$$J_{ion}(E_{ion}) = \exp\left(\frac{\mu - E_{ion}}{kT}\right). \tag{9}$$